Research Article Vol. 28, No. 6 / 16 March 2020 / Optics Express 8169
Optics EXPRESS

Genetic algorithm optimization of high order surface etched grating tunable laser array

MICHAEL J. WALLACE,[1,2,*] SEPIDEH T. NAIMI,[1] GAURAV JAIN,[1] ROBERT MCKENNA,[1] FRANK BELLO,[1] AND JOHN F. DONEGAN[1,2,3,4]

[1]School of Physics, Trinity College Dublin, Ireland
[2]Future Networks and Communications (CONNECT), Trinity College Dublin, Ireland
[3]Centre for Research on Adaptive Nanostructures and Nanodevices (CRANN), Trinity College Dublin, Ireland
[4]Advanced Materials and Bioengineering Centre (AMBER), Trinity College Dublin, Ireland
[*]wallacmj@tcd.ie

Abstract: A genetic algorithm is developed with a view to optimizing surface-etched grating tunable lasers over a large optimization space comprised of several variables. Using this approach, a new iteration of slotted lasers arrays are optimized showing significant improvements over previous designs. Output power, lower grating order, fabrication tolerance and performance at high temperatures are among key parameters improved. The new designs feature a much lower grating order (24-29) than used previously (37). The biggest improvement is a near doubling to slope efficiency to 0.1-0.13 mW/mA, with wavelengths from the array covering the C-band . The designs show a reduced sensitivity to etch depth variations. Designs with linewidths down to 100 kHz are also simulated. This algorithm can be readily applied to different wafer materials to efficiently generate slotted lasers designs at new wavelengths.

1. Introduction

Widely wavelength tunable lasers are key enablers of wavelength-division multiplexing (WDM) systems, with sampled grating distributed Bragg reflector (SG-DBR) [1] and distributed feedback (DFB) [2] laser arrays demonstrating wide tunability. Although tunable DFB and DBR lasers demonstrate good optical power and wavelength stability, the high-resolution processing and complex regrowth steps involved in their fabrication can result in low yield [3]. These complex manufacturing processes may be a barrier to the implementation of scalable fiber-to-the-x (FTTx) solutions, with architecture such as passive optical networks (PONs) requiring low-cost tunable lasers on the optical network unit (ONU) side [4]. To facilitate such systems, it would be advantageous to implement single-mode lasers with relatively simple fabrication; that is, with no regrowth and low cost etch processes. To this extent, laterally coupled DFB lasers and surface-grating DBR lasers that use a single growth step have been employed [5,6]. However, the patterning of these devices still requires electron-beam lithography, which itself is expensive and time consuming. A potential solution to this cost issue is to simplify the fabrication process even further by etching high order grating features on the surface of the waveguide, thereby avoiding the aforementioned high-resolution processing and regrowth steps. Such slotted lasers could be fabricated with high yield, and have been found to exhibit low threshold currents, narrow linewidths and modest slope efficiencies [3,7,8]. When combined with regrowth free passivisation methods, for example ion implantation as presented in [9], such lasers can potentially enable photonic integrated circuits (PICs).

The design and optimization of such surface grating based lasers in the literature tend to rely on an ad hoc approach, simulating grating properties such as reflectivity over a limited range of design variables and choosing a suitable grating. A generalized approach to surface grating optimization is lacking and to our knowledge an efficient method fully covering the various design

#383914 https://doi.org/10.1364/OE.383914
Journal © 2020 Received 21 Nov 2019; revised 24 Jan 2020; accepted 10 Feb 2020; published 5 Mar 2020

Optics EXPRESS

variables for a slotted high order grating while also encompassing the complexities introduced by them has not been demonstrated. As such, this paper sets out to define a method whereby slotted grating laser diodes can be rigorously optimized, taking all degrees of freedom into account while being applicable for arbitrary laser performance requirements. Optimization algorithms have been applied to a large number of photonic structures showing improved designs and operation [10–16]. Photonic devices including plasmonic absorbers, metasurfaces and photonic-bandgap structures have shown improved performance through the use of such optimization techniques.

2. Slotted grating laser design and operation

Figure 1 shows a schematic of the existing slotted laser structure featuring a surface-etched high order grating, which has been described in [7] and [8]. The 2 μm wide ridge waveguide is split into two sections: gain (back), grating (front). The front current controls the grating reflectivity peak (Bragg peak), the back controls the gain as well as the phase of the lasing mode, and the curved SOA section amplifies the signal while also forming part of the waveguide. The front section is fixed in length at 230 μm, while lasers of varying back section length have been developed, resulting in total cavity lengths of 400, 700 and 1000 μm. Figure 1(b) shows an optical image of the fabricated device, in which an SOA has been integrated for increased output power. Note the 200 μm SOA is curved at 7 to reduce the reflection from the front facet [7]. The front grating section has 24 slots in total, consisting of three distinct periods (labelled $\Lambda_{1,2,3}$). This non-uniform grating suppresses unwanted reflection peaks, which occur at one free spectral range (FSR), ~ 37 nm, as shown in 1(d). The three periods, which compose the grating, are ~ 8.5, 9.9 and 11.4 μm. The periods were previously optimized for high reflectivity using the scattering matrix method (SMM) [7].

A high reflectivity (HR) coating is applied to the back facet to improve threshold and slope efficiency and an anti-reflection (AR) coating is applied to the output facet to avoid feedback, Fig. 1(e). An array of 12 lasers with lasing wavelengths spanning 28.5nm is achieved by changing the pitch of each lasers' grating using the Bragg equation

$$p = \frac{m\lambda_{Bragg}}{2n_{eff}}, \tag{1}$$

where p is the grating period, m is the grating order n_{eff} is the effective index and λ_{Bragg} is the wavelength of the Bragg peak.

The epitaxial structure, shown inset in Fig. 1(c), contains an active region consisting of five AlGaInAs quantum wells with an emission peak at ~ 1545 nm. Above this are a 1.6 μm thick p-doped InP layer, 50 nm-thick, p-doped InGaAsP layer, and a 200 nm InGaAs contact layer. The laser fabrication process involves forming the ridge and slots via two inductively coupled plasma (ICP) etch steps using Cl_2 and N_2 gas, after which the laser ridge is passivated and metal contacted. The laser is subsequently coated in high reflection (HR) and anti-reflection (AR) films, before being eutectic bonded onto an AlN carrier. It should be noted that the lasers in the current study do in fact use e-beam lithography to form the grating patterns due to the lack of an i-line stepper in the foundry, but this is not a technical requirement of the device fabrication. These lasers have been found to exhibit strong performance under continuous wave (CW) operation. In previous work [3], an array of 12 slotted lasers demonstrated full C-band coverage and a threshold current of 25-35 mA at 20C, with a side-mode suppression-ratio (SMSR) > 40 dB and a linewidth below 500 kHz. Very recently, similar high order slotted lasers have been fabricated by optical lithography [8]. The optimizations will use the previously described design of the laser array as the basis for further iteration, i.e. the basic structure of a gain section and grating section; HR and AR coating, slotted gratings and the epitaxial structure will not be altered. Free variables in the optimization will include etch depth, grating period, number of periods, slot width and cavity length.

Optics EXPRESS

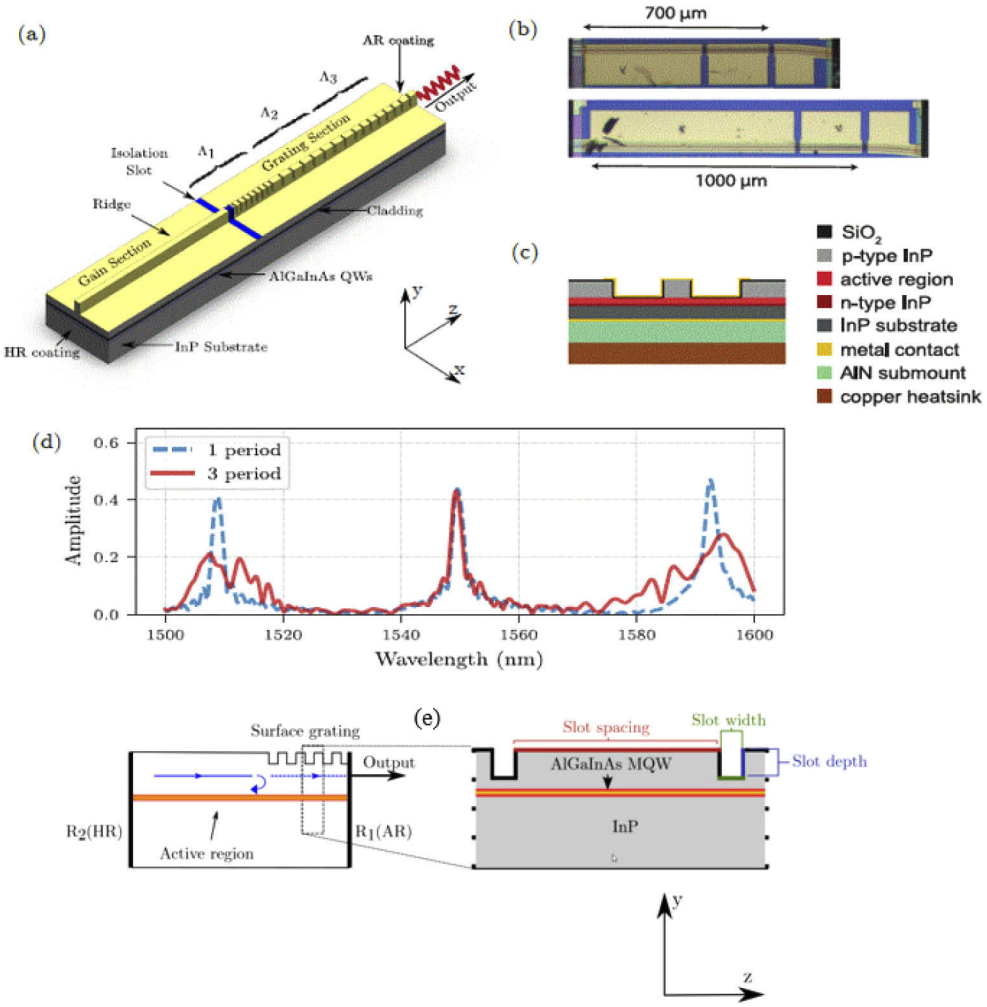

Fig. 1. High order slotted laser. (a) Schematic showing gain and grating sections with separate contacts. The grating here has three periods (b) optical image with contact to various sections and (c) epitaxy design of the laser, showing the ridge waveguide in the centre, (d) reflection spectrum of the 3 period grating (red, solid) compared with a single period (blue, dashed). (e) Schematic of the slotted grating laser with slot parameters indicated.

3. Optimization

Optimizing slotted laser diodes poses a number of challenges generally not encountered when optimizing lasers with buried gratings. Chief among these challenges is the fact that etching into the laser ridge necessarily introduces radiation loss, as a portion of the field profile will overlap with the etched slot and be radiated from the waveguide. As a result, the grating structure needs to be carefully optimized, and although one cannot entirely avoid loss, it is crucial to optimize the laser such that radiation loss is minimized, while also achieving sufficiently high reflectivity and narrow bandwidth from the Bragg peak.

In addition to radiation loss, mode competition from FSR reflection peaks introduces further complexity into the design of slotted lasers. A particular challenge arises from the fact that high order grating periods (~37^{th}), which from simulations are seen to coincide with high reflectivity,

Optics EXPRESS

have a relatively narrow FSR of ~ 40 nm. This narrow FSR results in adjacent reflection peaks competing with the main lasing mode, particularly at elevated temperatures where the gain peak may be detuned from the designed lasing wavelength. The reflection spectrum must be engineered such that these side peaks are either suppressed or are located at an appropriate wavelength not overlapping the gain spectrum.

As discussed above, previously, multiple period gratings have been employed to overcome competition from FSR reflection peaks. However, the question remains whether this is the most effective approach. Indeed, it may be more efficient to simply reduce the period order thereby increasing the FSR spacing. This approach may, however, have negative impacts on performance criteria such as linewidth, threshold, output power and SMSR. As such, it is necessary to formulate these criteria into an appropriate figure of merit (FOM) with which the genetic algorithm can evaluate an individual's overall fitness, and over the course of the optimization minimize.

3.1. Optimization procedure

If output power, SMSR and linewidth are evaluated to optimise the laser performance as functions of injection current, we can use the concept of an operating current, I_{op}. This operating current is defined as the minimum current for which all the specified performance criteria are met. This definition avoids the over optimization of certain performance criteria at the expense of others. The concept is illustrated in Fig. 2 for a hypothetical optimization problem in which we wish to optimize a laser with linewidth $\leq$ 2MHz, output power $\geq$ 7mW and SMSR $\geq$ 40 dB. A laser with the performance shown in Fig. 2(a), although capable of meeting the SMSR and linewidth requirements below 60mA, must nonetheless be biased at 100mA in order to achieve the desired output power. As such, the operating current is 100mA and the laser is not particularly well optimized — that is to say, the various performance criteria are not suitably balanced with one another in order to minimize the operating current. A better optimized laser is shown in Fig. 2(b), whereby SMSR and linewidth performance have been sacrificed (as would be the case when reducing mirror reflectivity) in order to increase the slope efficiency. As a result, all performance criteria are now met simultaneously at a lower injection current of 70mA, thus reducing the operating current I_{op} of the device. By basing the FOM which we are minimizing on the operating current, our optimization will naturally balance the performance targets against one another as shown in Fig. 2(b).

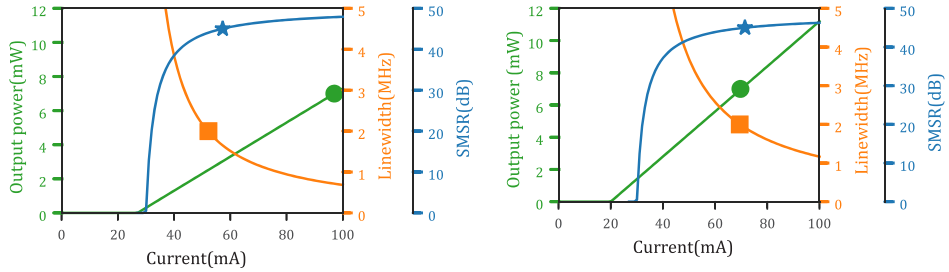

(a) Un-optimized case. (b) Optimized case.

Fig. 2. Illustration of laser optimization in terms of key parameters. (a) Shows the case where a particular laser is poorly optimized for a given set of minimum required performance, (b) shows the optimized case with a lower operating current required.

The temperature performance also needs to accounted for in the FOM. This is important for the laser array to operate well above room temperature. The simplest approach is to evaluate the lasing wavelength over the required temperature range and if the calculated lasing wavelength deviates from the wavelength designs at any temperature; set the FOM equal to a large value to

Optics EXPRESS

reduce the fitness of the individual. However, such discontinuous approaches can be deleterious to the convergence of the optimization.

Alternatively, we can describe the temperature performance in a manner such that individuals are punished proportional to the fraction of the temperature range they fail to cover. This is achieved by setting the FOM as

$$FOM = I_{op} + I_{op}(1-\eta_T)\cdot w, \tag{2}$$

where I_{op} is the operating current as previously defined and η_T is the fraction of the temperature range over which the correct lasing wavelength is maintained and w is a weighting parameter with which we can set the priority of covering the temperature range. The FOM which is being minimized, is now continuous and temperature stability is taken into account proportionally.

In order to optimize the laser diodes a genetic algorithm (GA) is implemented to minimize Eq. (1). The large number of variables and complex optimization space require an algorithm, which can converge in reasonable run times and is also capable of escaping local minima encountered in FOM. Figure 3 shows the general schematic of the genetic algorithm. The algorithm starts by seeding the population with a random set of individuals. This initial population may be seeded with designs, which are known to have good fitness values in order to help the optimization converge faster. Once an initial population is generated each individual is passed to the fitness function and a fitness value is returned. Once each individual within the population has a computed fitness value, a selection process removes individuals with low fitness. A tournament selection method is used whereby in each tournament, N individuals are selected at random from the population and the fittest individual is selected. A new generation of individuals is now created by randomly mutating a number of surviving individuals as well as randomly crossing over genes between a number of individuals. Once this new generation

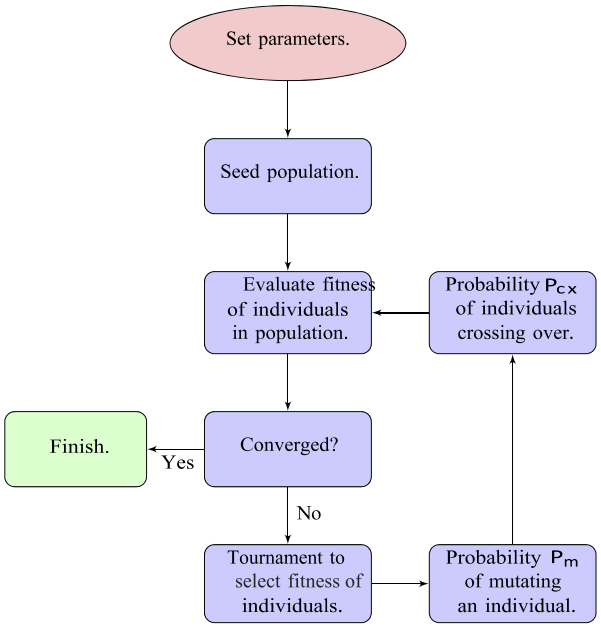

Fig. 3. Flowchart illustrating the genetic algorithm. Fitness is the figure of merit described in Eq. (2), tournament is the selection method used, gene refers to the free geometric variables in the optimization process and mutation represents a random alteration in an individuals gene.

Optics EXPRESS

has been defined, the individuals are once again evaluated for fitness and the process repeats until a satisfactory solution has been found. Care needs to be taken when defining each of the previously mentioned steps, which are now discussed in detail.

3.2. Evaluating performance criteria

As shown in Fig. 4, the performance criteria on which we will base our designs are output power, linewidth, SMSR and thermal performance. In order to accurately evaluate a given designs output power, the time-domain transfer matrix method (TD-TMM) is solved [17] and simulation parameters can be found in [18]. To reduce run time, we simply simulate the output power at two currents above threshold and as the output power is approximately linear, we use these two points to estimate slope efficiency and threshold. A similar approach is taken for the linewidth simulation where the photon density in the gain section at two currents above threshold is linearly fitted and subsequently used in the modified Schawlow-Townes linewidth equation given by

$$\Delta\upsilon_{FW} = \frac{(\Gamma R'_{sp})}{4\pi S}(1 + \alpha), \tag{3}$$

where S is the average photon density in the cavity (calculated via the TD-TMM), R'_{sp} is the spontaneous emission rate, and α is the linewidth enhancement factor [19]. This allows us to quickly calculate linewidth and output power values over a sufficient range of injection currents.

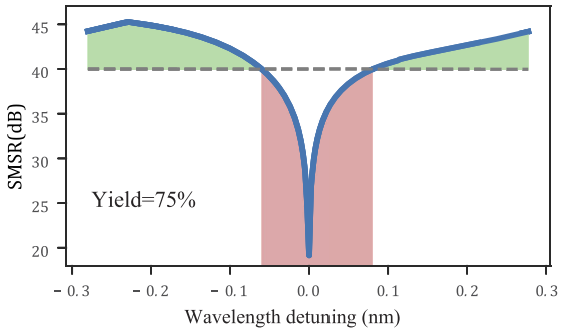

Fig. 4. Simulated SMSR versus wavelength detuning over one mode spacing. Red shading corresponds to SMSR below a defined minimum and green is above.

Although it is possible to calculate the SMSR via the TD-TMM, this requires a long run time in order to accurately simulate the side mode power. Furthermore, the issue of cleave error makes evaluating the SMSR performance somewhat more complicated, as the SMSR of a given laser will change as a function of cleave error. Due to this, we in fact choose to represent SMSR performance in terms of single-mode yield, i.e. the fraction of fabricated lasers, which under uniform current injection are expected to have an SMSR greater than a minimum value, due to variations in cavity length due to random cleave error.

The SMSR can be approximated using the equation

$$SMSR(1) \approx 10\, log_{10}\left(\frac{\Delta\alpha_m + \Delta g}{\delta_G} + 1\right), \tag{4}$$

where $\Delta\alpha_m$ is the difference between the lasing and competing modes mirror loss, Δg is the difference between the lasing and competing modes gain and δ_G can typically be taken as

$$\delta_G \sim 10^{-3}\,\frac{I_{th}}{I - I_{th}} \tag{5}$$

Optics EXPRESS

where I_{th} is the threshold current and I is the injection current [19]. The change in SMSR with cleave error is then calculated by shifting the wavelength of the longitudinal modes over one mode spacing. The percentage of SMSR greater than a defined minimum is the single mode yield. This calculation is performed for a range of currents such that the yield can be accounted for in the operating current, whereby a minimum defined yield must be obtained.

Finally, a laser design needs to be assessed for its performance over a range of temperatures. In order to assess the laser's temperature tuning, the lasing wavelength over a required temperature range can be calculated. This calculation is performed by obtaining the maximum of the round trip gain over a range of temperatures. The round trip gain is given as,

$$g_{round} = r_1(\lambda) \times r_2 e^{g(\lambda)L} \tag{6}$$

where $r_1(\lambda)$ and r_2 are the grating end facet reflectivities, respectively. $g(\lambda)$ and L are net gain and the laser cavity length [20]. The gain spectrum is taken to red-shift at 0.5 nmC^{-1} and the Bragg peak at 0.1nm°C^{-1}. From this, we can calculate the lasing wavelength from the maximum round trip gain of Eq. (6) over a range of temperatures. We define the maximum operating temperature as the highest temperature at which the maximum round trip gain coincides with the designed wavelength. The fraction of the desired temperature range which a laser achieves (η_T) is thus evaluated with the performance criteria evaluated we can now calculate and optimize the FOM from Eq. (1).

During the genetic optimization we will allow the following design parameters to vary (mutate): etch depth, grating period, number of sub periods, slot width and cavity length. The inclusion of multiple period gratings results in a very large number of possible grating structures. The number of possible gratings is limited by defining the grating in terms of *period number* and *period spacing*.

The period number defines the number of different periods within a grating while the period spacing defines the difference in period between each of these. This definition results in an equal number of slots for each individual period within the grating. For example, a multiple period grating G_T with period order = 30, period number = 3, period spacing = 5 and slot number = 30 would be composed of the sub-gratings shown in Table 1. For convenience, the gratings subsequently presented will be expressed in terms of period number and spacing, and will not be expanded into constituent gratings as in Table 1. The gratings can be expanded via

$$G_T = \sum_{i=0}^{n} (m_0 + (i\Delta m)) \frac{N}{n} \tag{7}$$

where m_0 is the period order, Δm is the period order spacing, n is the period number, and N is the total slot number [20]. The slot order m_s is related to the slot width Λ_s as follows:

$$\Lambda_s = (m_s) \frac{\lambda_{Bragg}}{2n_s} \tag{8}$$

where n_s is the effective index of the slotted region. The values typically used for the genetic algorithm parameters are shown in Table 2. The values were chosen through trial and error to provide a good rate of convergence and solutions. A mutation event refers to a specific design undergoing a random alteration; whereas a gene mutation refers to a specific parameter, such as etch depth, undergoing an alteration. Similarly, cross over probability is the chance of two designs undergoing a cross over event and gene cross over probability represents the probability of two parameter values being exchanged during said cross over event.

3.3. Results: Optimizing laser arrays

Previously, lasers arrays using a high-order grating have been designed with the goal of full C-band coverage from 1530 nm to 1565 nm [7]. Subsequent fabrication of these designs

Optics EXPRESS

Table 1. Example of a multiple period grating composition.

	G_1	G_2	G_3
Period order	30	35	40
Slot number	10	10	10

Table 2. Genetic algorithm parameters. N_g is the number of free varying genes.

Parameter	Value
Population size	$20 \times Ng$
Mutation event probability P_m	0.2
Gene mutation probability p_m	~ 0.15
Cross over probability C_{cx}	0.15
Gene cross over probability c_{cx}	0.1
Tournament size	3

yielded arrays with full C-band coverage, low linewidth and good SMSR. However, a number of outstanding issues remain with these designs. Primarily the laser arrays had lower output power than desirable. In addition, the longer cavity lasers of length 700 μm and 1000 μm used to reach lower linewidth had sub-optimal performance at elevated temperatures due to competition from the higher wavelength FSR reflection peak. With this in mind, we wish to use the genetic optimization process to overcome these issues.

In order to assess the effectiveness of the genetic algorithm it is instructive to directly compare a newly optimized array with previous arrays. One factor, which makes this difficult, is that many of the performance criteria in the previous optimization, such as slope efficiency and yield were not explicitly defined to the same degree as in the genetic optimization. However, one specific goal for the 700 μm laser array was to achieve ≤ 1 MHz linewidth, which can be used as a performance criterion to compare with. Thus, the operating current of the previous design is defined as the current at which 1 MHz linewidth is reached. The yield and output power at this operating current are then calculated for the array, and the average of these values is used as performance requirements for the genetic algorithm. The maximum designed operating temperature is taken as 40°C, which is the theoretical maximum operating temperature of the 1530 nm channel laser as calculated using Eq. (5) to evaluate the highest temperature at which the correct wavelength is maintained. In this way, the previously designed lasers are re-optimized with similar performance goals, allowing for a valid comparison. The cavity length is also set constant at 700 μm. This optimization, undertaken using the aforementioned conditions, will be referred to as *optimization 1* henceforth.

The performance parameters for optimization 1 may not be ideal for operation at 1 MHz, and as such these are primarily used as a method to compare with the previous design. A newly optimized design from scratch would naturally adjust the parameters in order to enforce higher performance of the resulting laser. With this in mind, the desired maximum operating temperature is increased to 70°C, minimum output power to 12.0 mW (~10 dBm) and the minimum yield to 75%. This optimization run will be referred to as *optimization 2*.

Finally, *optimization 3* is defined as identical to *optimization 2*, but with a reduced yield requirement equal to 25%. The reasoning behind this being that for multi-section lasers we have the ability to correct for cleave error via current tuning, reducing the requirement for high single mode yield [3].

Each array of lasers consists of 12 individual lasers each designed to operate at linearly spaced wavelengths from 1530 to 1565 nm in order to cover the C-band. Optimizing for a range of

Optics EXPRESS

wavelength lasers on a single chip imposes certain restrictions on our optimization parameters. As etching a different depth for each laser is not practical in terms of fabrication, it is necessary to first determine an ideal etch depth for the array. Additionally, as the chip has a set length, all lasers in the array must have the same length. In order to determine a set etch depth and cavity length for the entire array, the 1530 nm laser is first optimized, with the reasoning that this laser has in the past proved to have lower performance and was most susceptible to competition from FSR peaks at high temperatures [20]. Once an optimal etch depth and cavity length has been determined for the 1530 nm laser, these values are set as constant for all subsequent lasers in the array. The resulting etch depth and cavity length may not be optimal for the entire array; however, ensuring good performance for the 1530 nm channel laser is a priority — the laser array is only as good as its weakest performing laser. In order to shorten the convergence time for subsequent lasers in the array, each optimization is started by seeding the population with a small portion of individuals from the previous optimized laser in the array. As the wavelength channels are closely spaced, these seed individuals should in general be close to the optimal design for the laser being optimized.

3.3.1. Simulated performance

The performance of the re-optimized laser designs can be seen in Fig. 5. Optimization 1, which has the same theoretical performance requirements as the previous design, shows improvement in performance with an average increase of 45% for the slope efficiency, 62% for the output power at operating current, while the average operating current increases marginally by less than 1%. In both cases, the lasers have ≤ 1 MHz linewidth at their respective operating currents. Optimization 2, which has higher performance requirements is seen to have a significantly increased slope efficiency. As a higher output power requirement was defined, the operating current is also naturally higher, although the average increase in operating current of ~ 35% yields an average increase in output power of ~200%. The effect of reducing the yield requirement is

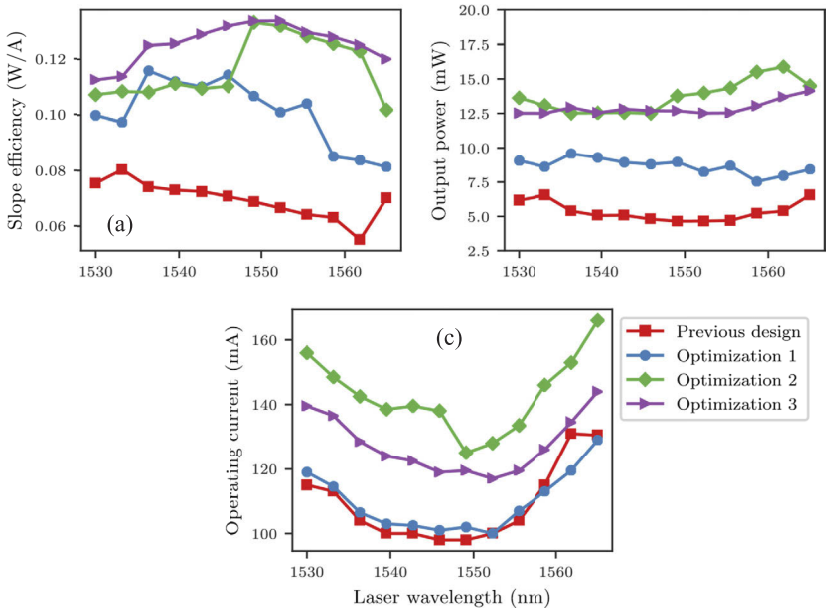

Fig. 5. Simulated performance of the optimized and previous laser arrays: slope efficiency (a), output power at respective operating current (b), operating current (c). Laser cavity length is 700μm

Optics EXPRESS

seen from Optimization 3, where the operating current is notably reduced and the slope efficiency is generally higher across the array. The increase in slope efficiency for Optimization 3 relative to Optimization 2 is a result of the genetic algorithm re-balancing the performance criteria, i.e. as a lower yield was allowed the algorithm was free to decrease the SMSR in favor of output power.

The genetic algorithm optimization also results in improved SMSR/single mode yield and temperature performance. Figure 6 compares the previous design yield and maximum operating temperature. The newly designed lasers have a consistent yield $\geq 70\%$ at 150 mA. The effect of explicitly defining a minimum temperature tuning range can also be seen. Optimization 1 and the previous design are seen to have a maximum simulated operating temperature of $\sim 40°C$ for the 1530 nm laser while optimization 2 has a theoretical maximum temperature of $\geq 70°C$. The spectral performance of the optimized laser is shown in Fig. 7.

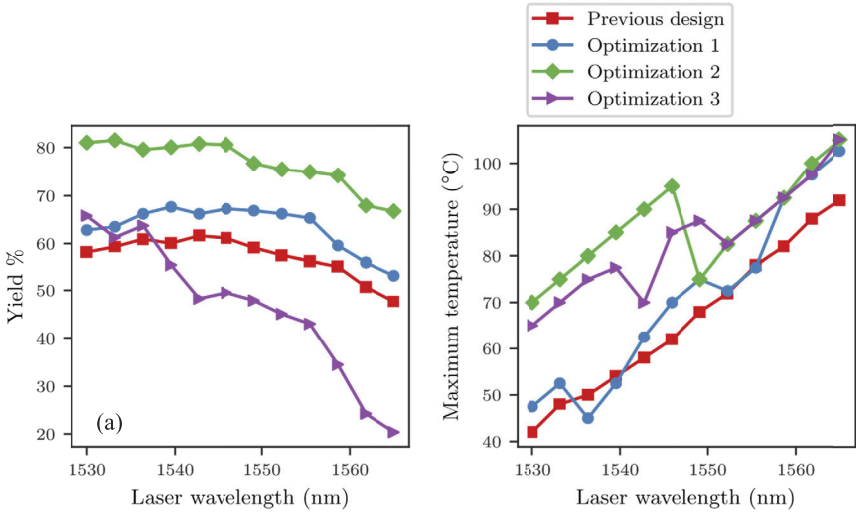

Fig. 6. Simulated performance of the previous 700 μm cavity length array design and the optimized design: single mode yield (a) and maximum operating temperature (b).

The top plot shows the simulated spectrum of the optimization 1 at 50°C and 65°C for the blue-most laser at 1530 nm and the lower plot shows the results from optimization 2 for the same conditions. The mode hop that occurs for the optimization 1 case is due to the gain peak red shifting. As the gain peak red shifts the next FSR reflection peak receives a higher round trip gain. If the gain peak red shifts enough, this peak will dominate over the intended peak. Therefore, a change in net modal gain for the individual reflection peaks caused by red shifting gain peak. The improved temperature performance of optimization 2 is due to the greater FSR in this particular design. In contrast, optimization 2 in which we explicitly set our required temperature tolerance to be $\geq 75°C$ shows markedly improved spectral properties at a heatsink temperature of 65°C, maintaining the designed wavelength channel. The newly optimized designs are able to achieve better thermal performance due to a lower order grating design. Optimization 2 resulted in gratings with a single 24^{th} order period in contrast to the previous 3 period grating ranging from 32^{nd} to 46^{th} order. The use of a lower order grating results in a larger FSR and as such, the design is less susceptible to mode competition from adjacent reflection peaks. Also note that the slot depth is significantly decreased from 1.35 μm to values varying from 1.1 μm to 1.2 μm. This has the effect of reducing the scattering loss and increasing the output power. The results for optimizations 1, 2 and 3 for the laser arrays are shown in Tables 3, 4, 5.

Optics EXPRESS

Table 3. Optimization 1.

Lasing Wavelength nm	1530	1533	1536	1540	1543	1546		1549	1552	1555	1559	1562	1565
Etch depth µm							1.195						
Slot number	31	31	26	26	31	31		31	27	27	32	31	31
Period order	28	28	36	36	29	29		29	35	35	28	28	28
Period number	2	2	1	1	1	1		1	1	1	1	1	1
Period spacing	1	1	–	–	–	–		–	–	–	–	–	–
Slot order							4.5						
Cavity length µm							700						
Slope efficiency W/A	0.100	0.097	0.116	0.112	0.110	0.114		0.107	0.101	0.104	0.085	0.084	0.081
Threshold mA	28.29	26	23.85	19.98	21.29	24.07		18.03	18.38	23.53	24.45	24.39	25.35
Operating current mA	119	114.5	106.5	103	102.5	101		102	100	107	113	119.5	129

Table 4. Optimization 2.

Lasing Wavelength nm	1530	1533	1536	1540	1543	1546		1549	1552	1555	1559	1562	1565
Etch depth µm							1.1						
Slot number	45	45	43	43	43	43		33	33	33	33	31	33
Period order	24	24	24	24	24	24		29	29	29	29	29	28
Period number	1	1	1	1	1	1		1	1	1	1	1	1
Period spacing	–	–	–	–	–	4		–	–	–	–	–	–
Slot order							4.5						
Cavity length µm							660						
Slope efficiency W/A	0.107	0.109	0.108	0.111	0.109	0.110		0.133	0.132	0.128	0.126	0.123	0.102
Threshold mA	29.01	27.97	26.81	25.86	24.85	24.72		21.6	22.01	21.68	22.48	23.73	23.58
Operating current mA	156	148.5	142.5	138.5	139.5	138		125	128	133.5	146	153	166

Table 5. Optimization 3- Lower single mode yield.

Lasing Wavelength nm	1530	1533	1536	1540	1543	1546		1549	1552	1555	1559	1562	1565
Etch depth µm							1.05						
Slot number	40	38	37	34	28	28		28	27	27	26	25	25
Period order	24	24	24	24	28	26		26	29	29	29	29	29
Period number	1	1	3	3	1	4		4	1	1	1	1	1
Period spacing	–	–	1	1	5	1		1	4	4	–	–	–
Slot order							4.5						
Cavity length µm							710						
Slope efficiency W/A	0.113	0.114	0.125	0.126	0.129	0.132		0.134	0.134	0.129	0.128	0.125	0.120
Threshold mA	28.39	26.64	25.03	24.14	23.1	22.74		24.61	23.42	22.81	24.08	25.07	26.28
Operating current mA	139.5	136.5	128.5	124	122.5	119		119.5	117	119.5	126	134.5	144

Optics EXPRESS

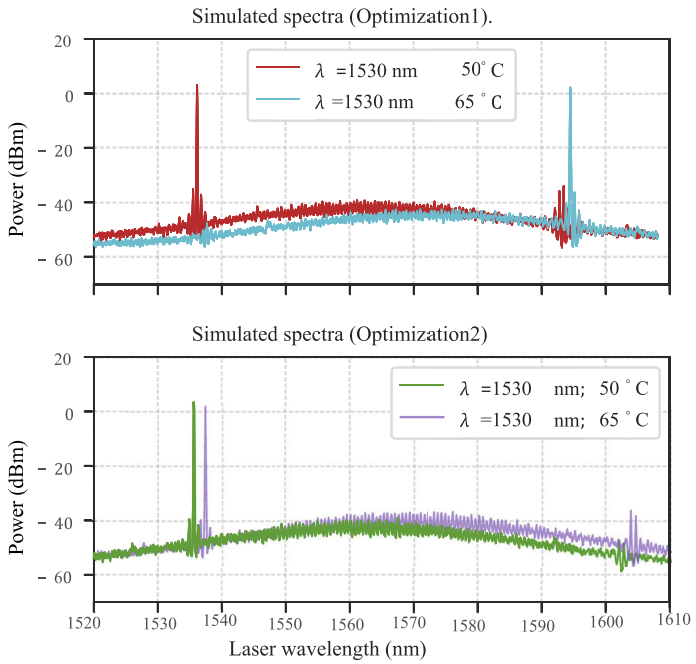

Fig. 7. Simulated lasing spectra of the optimized lasers showing improved thermal behaviour for optimization 2.

3.3.2. Results: Etch depth tolerance

Thus far, the performance improvements of explicitly defined parameters have been examined: output power, linewidth, yield and maximum temperature. Another aspect of design is fabrication tolerance. Simulations suggest that the etch depth in particular affects the performance of the laser, see Fig. 1(e). Figure 8 shows the fractional increase in operating current over a range of etch errors. Negative etch errors correspond to the slot being etched too shallow; while positive etch error corresponds to etching the slot deeper than intended.

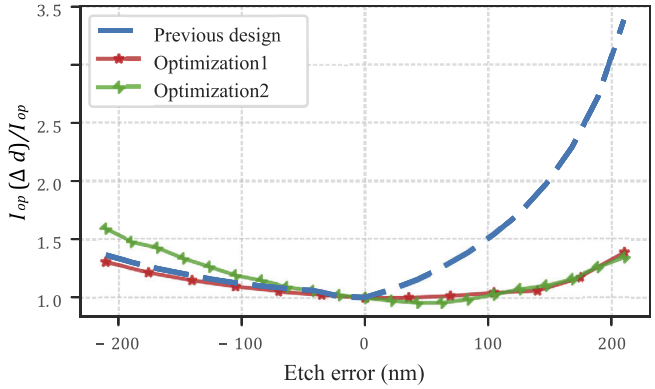

Fig. 8. Fractional increase in operating current versus etch depth error.

The simulation suggests that etching the slot too shallow has a relatively small effect on the operating current in all cases with optimization 2 being most sensitive to under etching of the

Optics EXPRESS

slot. In the case of an under etched slot the operating current is seen to increase due to reduced linewidth performance. For the original design, over-etching the slot is simulated to have a severe detrimental effect on the laser performance. A relatively small error of 100 nm in etch depth results in factor of 1.5 increase in operating current, and by 200 nm etch depth this factor increases to 3. In contrast, newly optimized designs are simulated to have a much greater tolerance to over etching of the slot depth.

Whether this improvement in fabrication tolerance is a result of the genetic algorithm is somewhat unclear. The nature of the genetic algorithm may indeed tend towards more tolerant design for a number of possible reasons, as the entirety of the optimization space is not covered, sharp peaks in fitness in the optimization space, which correspond to error sensitive designs may simply not be found by genetic algorithm. The genetic algorithm may account for fabrication tolerance to some degree, as individuals within a population, which are highly sensitive to changes in parameters such as, etch depth, and are more likely to lose fitness upon a maturation or cross over event. It may be the case that a primary downside of genetic algorithm approach, namely that the very best design in optimization space is not necessarily found, may in this case be beneficial. A key reason lower order gratings were not implemented in previous designs was the difficulty in finding such designs with sufficient reflectivity and transmission. The genetic algorithm has proven successful at locating such lower order designs.

3.4. Results: Low linewidth optimization

Advanced modulation formats with coherent detection are increasingly seen as an effective method of improving spectral efficiency. Such advanced modulation formats utilise phase-shift keying (PSK), a process whereby the carrier phase is modulated to encode data. As these modulation formats require the recovery of signal phase, certain minimum linewidths are required, with maximum data rates increasing with decreasing linewidth [21]. Table 6 shows the required linewidth in order to transmit at 40 Gbit/s for numerous modulation formats [22]. Thus far, we have optimized lasers arrays compatible with both 8PSK and Star 16QAM formats. For modulation formats such as 16PSK and Square 16QAM, however, substantially lower linewidths are required. The genetic algorithm can be utilised to evaluate the potential of slotted laser designs to reach suitable low linewidths and optimize a laser with this application in mind.

Table 6. Linewidth requirements for a range of modulation formats [22].

Modulation format	Minimum linewidth @ 40 Gbit/s
QPSK	10MHz
8PSK	1.6MHz
16PSK	240kHz
Star 16QAM	1.6MHz
Square 16QAM	120kHz
Square 64QAM	1.2kHz

As per the modified Schawlow-Townes equation [Eq. (3)], the laser linewidth can be reduced by increasing the power within the cavity and by reducing waveguide loss α_i. The latter is taken from previous measurements since we are not varying the wafer designs here. In order to increase the power within the cavity, another design parameter is allowed to vary during this optimization, namely the anti-reflective coating on the output facet. Increasing the facet reflectivity will increase the power within the cavity but will also reduce the slope efficiency and SMSR. Again, there is a need to balance various design parameters and performance criteria, which is achieved using the genetic algorithm. The convergence of the optimization can be seen in Fig. 9, which shows a 2D histogram of key parameters as they evolve through the optimization.

Optics EXPRESS

Solutions with cavity length < 1000 μm are quickly eliminated from the population. Gratings with an etch depth of ~ 1.2 μm are initially seen in the population but after generation 20 are replaced by shallower slot designs. The final design and performance is included in the Table 7. The resulting simulated linewidth is seen in Fig. 10(b). Simulations with a waveguide loss of $\alpha_i = 18\text{cm}^{-1}$ and $\alpha_i = 28\text{cm}^{-1}$ have been included, corresponding to the lower and higher ranges of experimentally measured values respectively [23]. For $\alpha_i = 28\text{cm}^{-1}$ a linewidth of ≤ 200 kHz can potentially be achieved at ~ 265 mA, opening up the potential for applications in 16PSK modulation systems. For $\alpha_i = 18\text{cm}^{-1}$ the simulation suggests that the minimum linewidth for Square 16QAM of ≤ 120 kHz can be achieved at ~ 265 mA. The lasing spectrum of the optimized design is also simulated in Fig. 11. The increase in facet reflectivity is not seen to significantly affect the lasing spectrum with an SMSR of ~ 48 dB being predicted at 260 mA. Although a relatively low power of 5 mW was specified for the design, the final design far exceeds this with a slope efficiency of ~ 0.078 W/A giving an output power of ~ 16 mW at 25°C under 265 mA injection current.

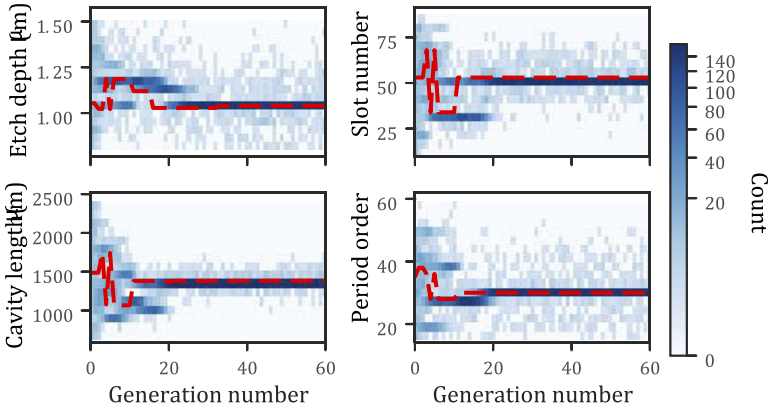

Fig. 9. Distribution of parameters during optimization of a low linewidth laser. Red line represents parameters of the best individual in a given generation.

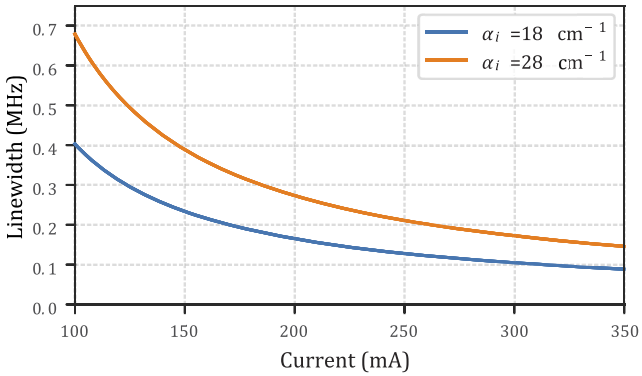

Fig. 10. Simulated linewidth of the optimized design. A waveguide loss of 28cm^{-1} used in the optimization corresponds to the most recent waveguide loss measurement; waveguide loss of 18cm^{-1} corresponds to the lowest waveguide loss, which has been measured for our devices.

Optics EXPRESS

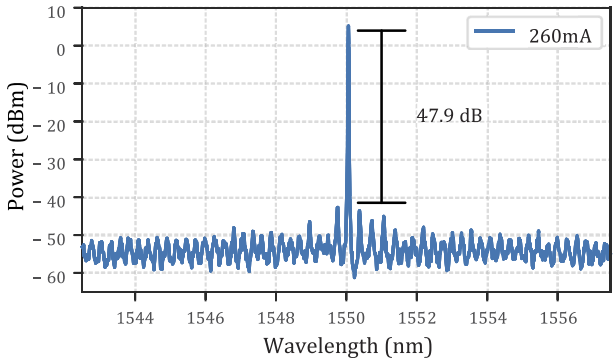

Fig. 11. Simulated lasing spectrum for low linewidth laser, biased at 265 mA.

Table 7. Optimization results for low linewidth laser.

Lasing Wavelength nm	1550
Etch depth (μm)	1.039
Slot number	53
Period order	30
Period number	1
Period spacing	-
Slot order	4.5
Cavity length (μm)	1381
AR reflectivity	0.169
Slope efficiency W/A	0.078
Operating Current mA	266.5
Threshold mA	35.81

4. Conclusion

Challenges inherent in designing and optimizing slotted laser diodes have been examined. In order to overcome these obstacles, a genetic algorithm has been implemented and the optimization problem for slotted lasers formulated accordingly. This results in an optimization where explicit performance requirements are balanced with one another in order to design a laser which achieves said requirements at the lowest possible injection current. A new iteration of laser arrays has been designed to improve upon the previously reported $700\mu m$. For such laser arrays, a shallower etch depth of $1.1\mu m$ was found to be optimal for increasing slope efficiency. This shallower etch depth is also predicted to improve tolerance to errors in etch depth. Notably, the laser arrays are re-optimized to have significantly improved performance at elevated temperatures and are simulated to maintain single mode performance at heatsink temperatures of up to 65°C.

Furthermore, the feasibility of slotted lasers with more niche performance requirements were investigated. A laser for low linewidth applications was optimized using the genetic algorithm. Simulations suggest that the optimized design is capable of sub 200kHz linewidth, with an SMSR$\sim$ 48 dB and a slope efficiency of $\sim$ 0.078 W/A. This performance was found to be comparable with similar surface etched grating lasers [23].

The algorithm presented can be used in future for efficiently generating designs for specific performance requirements. Moreover, the algorithm can be adapted to different wafer materials and used to generate new slotted laser designs for different operating wavelengths.

Optics EXPRESS

Funding

Science Foundation Ireland (15/IA/2854, CONNECT 13/RC/2077); H2020 Marie Skłodowska-Curie Actions (713567).

Disclosures

The authors declare no conflicts of interest.

References

1. V. Jayaraman, Z.-M. Chuang, and L. A. Coldren, "Theory, design, and performance of extended tuning range semiconductor lasers with sampled gratings," IEEE J. Quantum Electron. **29**(6), 1824–1834 (1993).
2. H. Ishii, K. Kasaya, H. Oohashi, Y. Shibata, H. Yasaka, and K. Okamoto, "Widely wavelength-tunable DFB laser array integrated with funnel combiner," IEEE J. Sel. Top. Quantum Electron. **13**(5), 1089–1094 (2007).
3. A. Abdullaev, Q. Lu, W. Guo, M. J. Wallace, M. Nawrocka, F. Bello, A. Benson, J. O'Callaghan, and J. F. Donegan, "Improved performance of tunable single-mode laser array based on high-order slotted surface grating," Opt. Express **23**(9), 12072–12078 (2015).
4. J. Zhu, A. Wonfor, S. H. Lee, S. Pachnicke, M. Lawin, R. V. Penty, J.-P. Elbers, R. Cush, M. J. Wale, and I. H. White, "Athermal colorless C-band optical transmitter system for passive optical networks," J. Lightwave Technol. **32**(22), 4253–4260 (2014).
5. D. Hofstetter, H. Zappe, J. Epler, and J. Sochtig, "Single-growth-step GaAs/AlGaAs distributed Bragg reflector lasers with holographically-defined recessed gratings," Electron. Lett. **30**(22), 1858–1859 (1994).
6. R. Martin, S. Forouhar, S. Keo, R. Lang, R. Hunsperger, R. Tiberio, and P. Chapman, "CW performance of an InGaAs-GaAs-AlGaAs laterally-coupled distributed feedback (LC-DFB) ridge laser diode," IEEE Photonics Technol. Lett. **7**(3), 244–246 (1995).
7. Q. Lu, W.-H. Guo, D. Byrne, and J. Donegan, "Design of slotted single-mode lasers suitable for photonic integration," IEEE Photonics Technol. Lett. **22**(11), 787–789 (2010).
8. M. J. Wang, H. L. Wang, P. J. Ma, F. X. Dong, A. J. Liu, and W. H. Zheng, "Eight-channel laser array with 100 GHz channel spacing based on surface-slotted structures fabricated by standard lithography," Opt. Lett. **43**(20), 4867–4870 (2018).
9. Q. Lu, W. Guo, A. Abdullaev, M. Nawrocka, J. O'Callaghan, M. Lynch, V. Weldon, and J. Donegan, "Re-growth free single mode lasers based on slots suitable for photonic integration," in *Transparent Optical Networks (ICTON), 2012 14th International Conference on*, (2012), pp. 1–4.
10. J. S. Parker, A. Sivananthan, E. Norberg, and L. A. Coldren, "Regrowth-free high-gain InGaAsP/InP active-passive platform via ion implantation," Opt. Express **20**(18), 19946–19955 (2012).
11. J. Goh, I. Fushman, D. Englund, and J. Vučković, "Genetic optimization of photonic bandgap structures," Opt. Express **15**(13), 8218–8230 (2007).
12. D. F. Rêgo, I. L. G. de Souza, and V. Felix Rodriguez-Esquerre, "Ultra-broadband plasmonic groove absorbers for visible light optimized by genetic algorithms," OSA Continuum **1**(3), 796–804 (2018).
13. S. D. Campbell, D. Sell, R. P. Jenkins, E. B. Whiting, J. A. Fan, and D. H. Werner, "Review of numerical optimization techniques for meta-device design [Invited]," Opt. Mater. Express **9**(4), 1842–1863 (2019).
14. Z. Li, L. Stan, D. A. Czaplewski, X. Yang, and J. Gao, "Broadband infrared binary-pattern metasurface absorbers with micro-genetic algorithm optimization," Opt. Lett. **44**(1), 114–117 (2019).
15. Y. Huang, Z. Zhen, Y. Shen, C. Min, and G. Veronis, "Optimization of photonic nanojets generated by multilayer microcylinders with a genetic algorithm," Opt. Express **27**(2), 1310–1325 (2019).
16. J. C. C. Mak, Q. Wilmart, S. Olivier, S. Menezo, and J. S. Poon, "Silicon nitride-on-silicon bi-layer grating couplers designed by a global optimization method," Opt. Express **26**(10), 13656–13665 (2018).
17. M. Davis and R. O'Dowd, "A new large-signal dynamic model for multielectrode DFB lasers based on the transfer matrix method," IEEE Photonics Technol. Lett. **4**(8), 838–840 (1992).
18. M. J. Wallace, R. O'Reilly Meehan, R. Enright, F. Bello, D. McCloskey, B. Barabadi, E. N. Wang, and J. F. Donegan, "Athermal operation of multi-section slotted tunable lasers," Opt. Express **25**(13), 14414 (2017).
19. L. Coldren, S. Corzine, and M. Mashanovitch, *Diode Lasers and Photonic Integrated Circuits, Wiley Series in Microwave and Optical Engineering* (Wiley, 2011).
20. A. Abdullayev, "Characterization of single-mode laser and tunable laser array based on etched high order surface gratings," Ph.D. thesis, Trinity College Dublin (2014).
21. K. Gao, J. Wang, L. Yang, X. He, D. Peterson, and Z. Pan, "Local oscillator linewidth limitation on 16 QAM coherent optical transmission system," in *CLEO/QELS: 2010 Laser Science to Photonic Applications*, pp. 1–2, (2010).
22. M. Seimetz, "Laser linewidth limitations for optical systems with high-order modulation employing feed forward digital carrier phase estimation," in *OFC/NFOEC 2008 - Conference on Optical Fiber Communication/National Fiber Optic Engineers Conference*, pp. 1–3, (2008).
23. M. Nawrocka, "Design and characterization of widely tunable semiconductor lasers based on etched slots," Ph.D. thesis, Trinity College Dublin (2014).